# Comparison of Three Key Marine Shale Reservoirs in the Southeastern Margin of the Sichuan Basin, SW China

**Jun Liu [1,2,3], Yanbin Yao [1,2,3,*]** (ID)**, Dameng Liu [1], Zhejun Pan [4] and Yidong Cai [1]**

[1] School of Energy resource, China University of Geosciences, Beijing 100083, China; darkhell@126.com (J.L.); dmliu@cugb.edu.cn (D.L.); yidong.cai@cugb.edu.cn (Y.C.)

[2] Coal Reservoir Laboratory of National Engineering Research Center of CBM Development & Utilization, China University of Geosciences, Beijing 100083, China

[3] Key Laboratory of Shale Gas Exploration and Evaluation, Ministry of Land and Resources, China University of Geosciences, Beijing 100083, China

[4] CSIRO Energy Business Unit, Private Bag 10, Clayton South, VIC 3169, Australia; zhejun.pan@csiro.au

* Correspondence: yyb@cugb.edu.cn

**Abstract:** This study performs a comprehensive comparison of three key marine shale reservoirs in the southeastern margin of the Sichuan Basin, and explains why commercial gas production was only achieved in the Lower Silurian Longmaxi (LSL) and Upper Ordovician Wufeng (UOW) formations, but not in the Lower Cambrian Niutitang (LCN) formation. The experimental methods included in situ gas content and gas composition tests, methane adsorption analysis, low-pressure $N_2$ adsorption, field emission scanning electron microscopy (FE-SEM), and total organic carbon (TOC) and vitrinite reflectance ($R_o$) analyses to evaluate the lithology, mineralogy, physical properties of the reservoir, organic geochemistry, in situ gas content and methane adsorption capacity characteristics of the three shales. The LCN shale has lower quartz and clay mineral contents and a low brittleness index, but higher contents of feldspar, pyrite and carbonate minerals than the LSL and UOW shales. The porosity and permeability of the LSL and UOW shales are higher than those of the LCN shale. The primary contributions to the high permeability in the LSL shale are its well-developed fractures and organic matter pores. In contrast, the over-mature LCN shale is unfavorable for the development of organic pores and fractures. Although the LCN shale has a higher methane sorption capacity than the LSL and UOW shales, the gas content and methane saturation of the LCN shale are distinctly lower than those of the LSL and UOW shales. This is primarily due to gas migration from the LCN shale, resulting from the activities of tectonic uplift and the unconformable contact between the LCN shale and the Dengying formation. When compared with gas shale in North America, the LSL shale is the most favorable shale reservoir out of the three Sichuan shales, while the combination of the LSL and UOW shales is also potentially productive. However, the individual single layer production of the UOW or LCN shales is still limited due to poor resource potential and/or reservoir physical characteristics in the study area.

**Keywords:** Lower Silurian Longmaxi formation; shale mineralogy; Upper Ordovician Wufeng formation; organic matter; shale gas content

## 1. Introduction

Shale gas is a form of unconventional natural gas that is found trapped within shale formations, which are composed of fine-grained sedimentary rocks and can be rich sources of conventional petroleum and natural gas [1,2]. The shale gas potential has been investigated in many countries,

of which only the United States, Canada, China, and Argentina have obtained commercial shale gas production. In 2015, the United States' shale gas production accounted for more than half of its domestic natural gas production, with a rate of 37 Bcf/d ($1.05 \times 10^5$ m$^3$/d), while production was only 0.5 Bcf/d ($1.42 \times 10^3$ m$^3$/d) in China, despite China holding the largest shale gas reserves in the world, with an estimated amount of technically recoverable shale gas of 1115.2 Tcf ($3.16 \times 10^{13}$ m$^3$) [3]. To meet energy demand, China is vigorously promoting shale gas exploration and is expecting accelerated development. To date, the breakthrough in Chinese shale gas has primarily occurred in the marine shales of southern China, particularly in the southeastern Sichuan Basin and its periphery, where the commercial production of shale gas has been achieved [4,5].

In the southeastern margin of the Sichuan Basin, there are three key marine formations for potential shale gas [6,7], namely, the Lower Silurian Longmaxi (LSL), the Upper Ordovician Wufeng (UOW) and the Lower Cambrian Niutitang (LCN) formations. Until now, commercial exploitation of shale gas has been achieved only in the LSL and UOW shales. However, no commercial gas has been obtained from the LCN shale, even though it is extremely thick and continuous in southern China [5,8].

Significant research has been performed relating to the shale gas development of the marine shales within and around the southeastern Sichuan Basin. According to these studies, the three organic-rich shales were formed in a low-energy, anoxic marine environment during different periods, and the sedimentation of the LCN shale was slightly affected by submarine hydrothermal activity [9,10]. The three shales have high TOC and a high potential for hydrocarbon generation, with the highest TOC content found in the LCN shale at 9.83 wt % [11,12]. The porosity and permeability of these shales are ultra-low, making the resources unrecoverable without hydraulic fracturing or other stimulation processes [12–14]. Methane in these shales is mainly stored in the adsorbed phase in organic matter and clay minerals, in the free phase in pores and fractures, and possibly in the dissolved phase in oil and water [15,16]. The contribution of adsorbed gas to the total gas content is 40%–85% for the LSL and UOW shales, compared to approximately 20%–80% for the LCN shale [17,18]. These previous investigations provide a comprehensive understanding of these shales. However, to the best of our knowledge, no systematic comparisons of the origin, standard characteristics, and shale gas potential have been made for the three marine shales in the southeastern margin of the Sichuan Basin.

This study compares the differences in lithology, mineralogy, reservoir physical properties, organic geochemistry, in situ gas content and methane adsorption capacity characteristics of the three marine shales (LSL, UOW and LCN) through data collected from field and laboratory experiments. The primary objective is to explore the factors influencing potential shale gas production in these shales. This study is also important for providing insight into the further development of shale gas in this region.

## 2. Geological Setting

The Sichuan Basin, one of the major gas-producing areas in China, with a total area of nearly $18 \times 10^4$ km$^2$, is a large intracratonic sedimentary basin and asymmetric tectonic depression located in southwestern China. The Sichuan Basin first subsided in the Late Proterozoic (Ediacaran) and has experienced a long, complex and multiphased subsidence and tectonic history that continues through to the present [19].

The study area is located in the southeastern margin of the Sichuan Basin (Figure 1). Geographically, it covers Fuling, Pengshui, Youyang, and Xiushan counties. This area has undergone multiple stages of tectonic activity, including the Caledonian orogeny (542–386 Ma), Hercynian orogeny (386–257 Ma), Indo-China movement (257–205 Ma), Yanshan movement (205–65 Ma) and Himalayan orogeny (beginning 65 Ma) [20,21]. This multistage tectonism was responsible for the complexities of the geological setting, such as numerous faults (some now active), universally steep dips and high tectonic stress [20]. Regarding the litho-stratigraphy of the study area, there are three typical marine shale formations, which from the top to the bottom consist of the LSL, UOW and LCN (Figure 2). The topmost shale is the LSL, with a thickness ranging from 35 m to 200 m and a maximum burial depth of

4900 m [21]. The UOW lies beneath the LSL and forms a conformable contact with the overlying LSL (Figure 2). The thickness of the UOW varies from 3 m to 10 m [22]. The LCN, located at the bottom of the Cambrian strata, possesses a maximum burial depth of 5500 m and a thickness of approximately 20–120 m [10]. The sedimentary center of the LSL and UOW is located in the northern study region, while that of the LCN lies in the south of the study area [9,10]. Therefore, the LSL and UOW are thicker in the central and northern study region than in the southern study region, whereas the LCN is thicker in the southern study region (Figure 1).
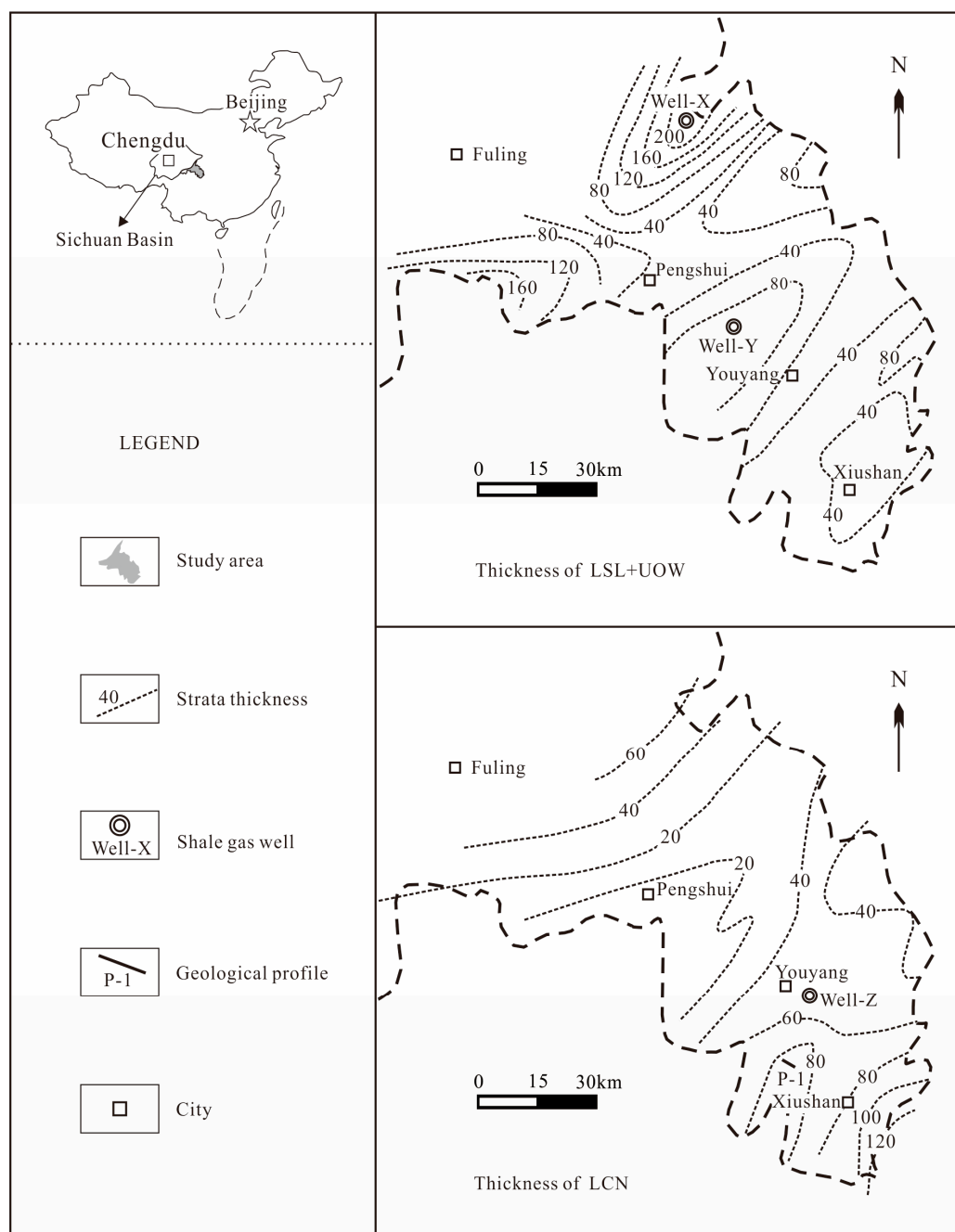


**Figure 1.** Regional overview of marine shales and sampling locations in the southeastern margin of the Sichuan Basin (modified from Liu et al. [10]).
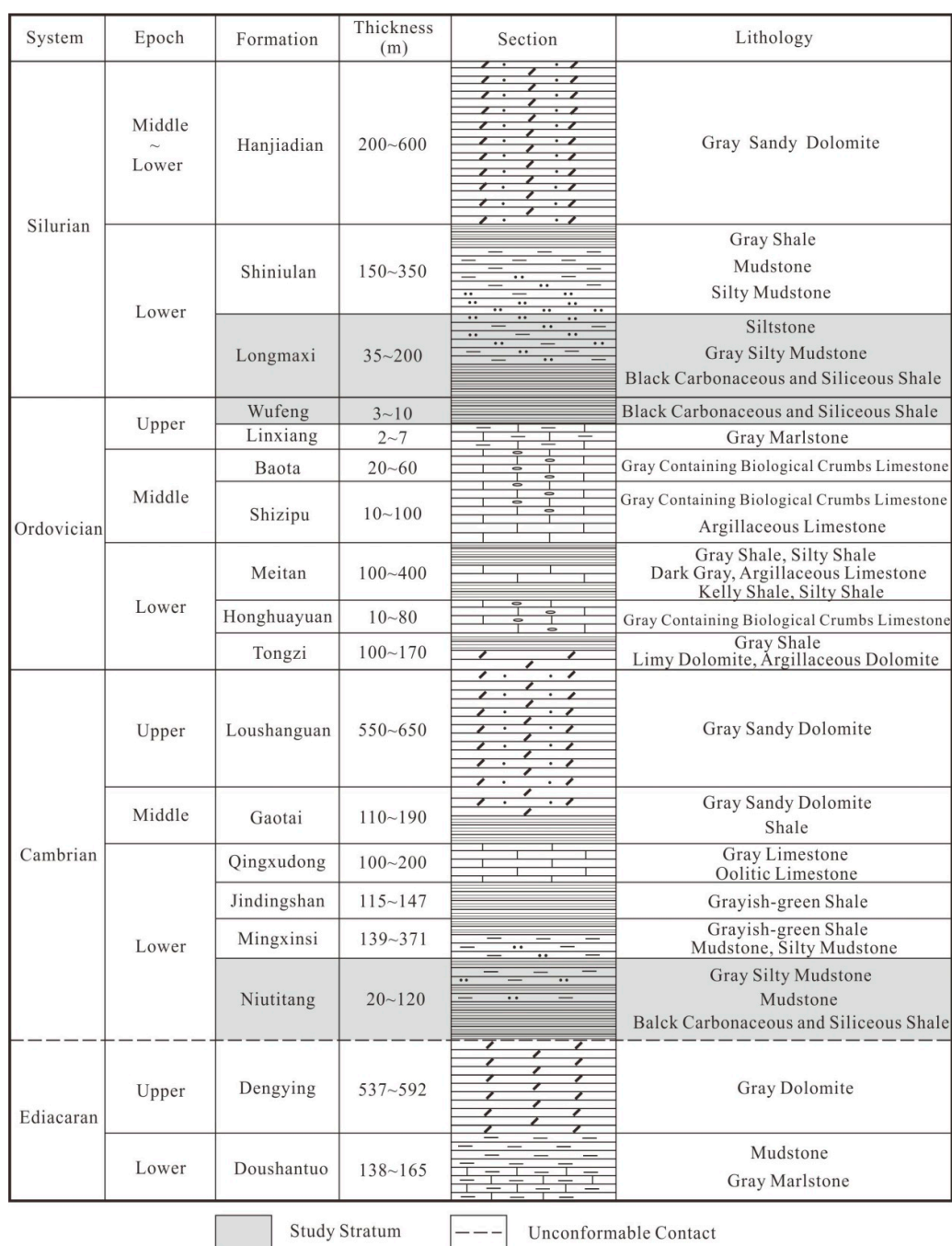
| System | Epoch | Formation | Thickness (m) | Section | Lithology |
|---|---|---|---|---|---|
| Silurian | Middle ~ Lower | Hanjiadian | 200~600 | | Gray Sandy Dolomite |
| | Lower | Shiniulan | 150~350 | | Gray Shale Mudstone Silty Mudstone |
| | | Longmaxi | 35~200 | | Siltstone Gray Silty Mudstone Black Carbonaceous and Siliceous Shale |
| Ordovician | Upper | Wufeng | 3~10 | | Black Carbonaceous and Siliceous Shale |
| | | Linxiang | 2~7 | | Gray Marlstone |
| | Middle | Baota | 20~60 | | Gray Containing Biological Crumbs Limestone |
| | | Shizipu | 10~100 | | Gray Containing Biological Crumbs Limestone Argillaceous Limestone |
| | Lower | Meitan | 100~400 | | Gray Shale, Silty Shale Dark Gray, Argillaceous Limestone Kelly Shale, Silty Shale |
| | | Honghuayuan | 10~80 | | Gray Containing Biological Crumbs Limestone |
| | | Tongzi | 100~170 | | Gray Shale Limy Dolomite, Argillaceous Dolomite |
| Cambrian | Upper | Loushanguan | 550~650 | | Gray Sandy Dolomite |
| | Middle | Gaotai | 110~190 | | Gray Sandy Dolomite Shale |
| | Lower | Qingxudong | 100~200 | | Gray Limestone Oolitic Limestone |
| | | Jindingshan | 115~147 | | Grayish-green Shale |
| | | Mingxinsi | 139~371 | | Grayish-green Shale Mudstone, Silty Mudstone |
| | | Niutitang | 20~120 | | Gray Silty Mudstone Mudstone Balck Carbonaceous and Siliceous Shale |
| Ediacaran | Upper | Dengying | 537~592 | | Gray Dolomite |
| | Lower | Doushantuo | 138~165 | | Mudstone Gray Marlstone |

▨ Study Stratum          - - - Unconformable Contact

**Figure 2.** Integrated stratigraphic column of the southeastern margin of the Sichuan Basin.

## 3. Materials and Methods

A total of twelve shale samples were collected from three exploration wells and a newly excavated sedimentary outcrop where the weathered surface was completely removed. The LSL shales and UOW shales are from Well-X and Well-Y, and the LCN shales are from Well-Z and the P-1 geological profile (Figure 1). The LSL shale samples from Well-X were labeled as "X-L-1" (the upper sample) and "X-L-2" (the lower sample), and other samples were labeled following a similar numbering rule (Table 1).

**Table 1.** Characteristics of the collected shale samples.

| Sample ID | Sampling Point | Strata | TOC (%) | $R_o$ (%) | Porosity (%) | Permeability ($10^{-3}$ mD) | BI (%) | Mineral Composition (wt %) | | | | | $V_L$ (m³/t) |
|---|---|---|---|---|---|---|---|---|---|---|---|---|---|
| | | | | | | | | Q | F | C | Py | Cly | |
| X-L-1 | Well-X | LSL | 2.93 | 3.12 | 2.78 | 1.21 | 61.5 | 55.7 | 7.2 | 3.2 | 2.3 | 31.6 | 1.090 |
| X-L-2 | Well-X | LSL | 3.51 | 4.01 | 3.02 | 1.42 | 71.0 | 61.9 | 8.9 | 2.9 | 3.9 | 22.4 | 3.263 |
| Y-L-1 | Well-Y | LSL | 3.02 | 2.44 | 3.37 | 2.11 | 58.8 | 53.3 | 7.7 | 7.5 | 1.6 | 29.9 | 2.077 |
| Y-L-2 | Well-Y | LSL | 3.64 | 2.83 | 3.11 | 1.72 | 52.1 | 46.1 | 8.1 | 6.3 | 3.4 | 36.1 | 3.999 |
| X-W-1 | Well-X | OUW | 3.58 | 2.75 | 2.99 | 1.33 | 32.2 | 27.8 | 10.9 | 7.2 | 2.8 | 51.3 | 3.464 |
| X-W-2 | Well-X | OUW | 3.17 | 2.97 | 3.43 | 1.86 | 67.0 | 59.7 | 7.9 | 2.9 | 3.0 | 26.5 | 2.457 |
| Y-W-1 | Well-Y | OUW | 4.08 | 3.11 | 3.11 | 1.40 | 72.6 | 64.2 | 7.4 | 3.4 | 4.2 | 20.8 | 2.855 |
| Y-W-2 | Well-Y | OUW | 3.36 | 2.22 | 2.20 | 0.98 | 54.7 | 49.8 | 5.2 | 13.1 | 3.7 | 28.2 | 4.198 |
| Z-N-1 | Well-Z | LCN | 5.65 | 3.68 | 2.61 | 1.55 | 56.7 | 47.1 | 13.3 | 20.5 | 3.7 | 15.4 | 4.846 |
| Z-N-2 | Well-Z | LCN | 7.53 | 4.27 | 1.25 | 1.01 | 54.0 | 44.2 | 11.5 | 7.1 | 6.6 | 30.6 | 7.441 |
| P-N-1 | P-1 | LCN | 4.59 | 3.91 | 2.23 | 1.34 | 46.1 | 41.0 | 7.9 | 18.3 | 3.1 | 29.7 | 4.590 |
| P-N-2 | P-1 | LCN | 6.88 | 4.31 | 1.09 | 0.87 | 45.1 | 37.5 | 12.3 | 11.9 | 4.6 | 33.7 | 6.106 |

NOTE: LSL—Lower Silurian Longmaxi formation; UOW—Upper Ordovician Wufeng formation; LCN—Lower Cambrian Niutitang formation; TOC—total organic carbon; $R_o$—vitrinite reflectance; BI—brittleness index; Q—quartz; F—feldspar; C—carbonate minerals; Py—pyrite; Cly—clay minerals; $V_L$—Langmuir volumes. BI = Q/(Q + C + Cly) × 100% (Jarvie et al. [1]).

All core samples were collected using a sealed coring process. To measure the in situ gas content, the steps for each operation were recorded during the coring process, including the beginning of core barrel extraction, when the barrel reached the surface and when the core was placed into the desorption canister. The detailed procedures of Hartman et al. [23] were adopted for the measurement of in situ gas content. The total in situ gas content consists of lost gas, desorbed gas and residual gas. The on-site desorbed gases from the desorption canisters were used to analyze the molecular components (e.g., $CH_4$, $C_2H_6$, $N_2$ and $CO_2$). The gas molecular components were analyzed using a gas chromatograph equipped with a flame ionization detector and a thermal conductivity detector, and subsequently corrected for the bulk compositional analyses of oxygen. In this study, gas content and composition tests were not made for the two outcrop samples.

The shale core and outcrop samples were analyzed for mineral composition, porosity, permeability, pore size distinction (PSD), TOC, vitrinite reflectance ($R_o$), methane adsorption capacity and field emission scanning electron microscopy (FE-SEM) observations. The mineral composition was investigated by X-ray diffraction (XRD) using shale powders (with an average grain size of 100 mesh) at 40 kV and 40 mA using Cu K$\alpha$ radiation. The semi-quantitative relative percentage of each mineral component was estimated using the method of Chalmers and Bustin [24]. The porosity of shale was analyzed by helium pycnometry, and the helium gas permeability was measured under overburden pressure. The permeability measurement was performed at a pore pressure of 250 psi and a confining pressure of 500 psi. For the PSD, a low-pressure $N_2$ adsorption experiment was employed at 77 K using the Barrett–Joyner–Halenda (BJH) analytical method. The TOC content was determined using a carbon sulfur analyzer after the tested sample was treated with hydrochloric acid to remove the carbonates. The $R_o$ was indirectly derived from bitumen reflectance due to the lack of vitrinite in marine shales using the equation reported by Jacob [25]. The methane adsorption capacity of the study shales was determined at 30 °C and with pressures up to 11 MPa, using Langmuir theory.

## 4. Results and Discussion

### 4.1. Lithology and Mineralogy

All samples collected from the LSL, UOW, and LCN can be described as black carbonaceous shale (Figure 3). Graptolites such as *Akidograptus* and *Monograptus* were common in the LSL and UOW samples (Figure 3a,b), but not in the LCN shales. This is a key characteristic distinguishing the LCN shale from the LSL and UOW shales.
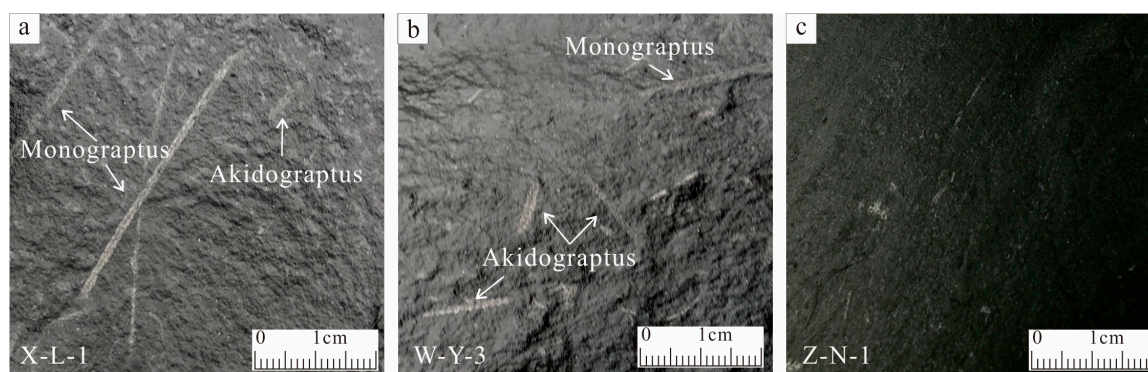


**Figure 3.** The lithological characteristics of the collected samples: (**a**) graptolites in LSL shale; (**b**) graptolites in UOW shale; (**c**) pure LCN shale.

The mineralogical analyses of the study shales are presented in Table 1 and Figure 4. The mineralogy of all collected samples is similar: all samples are dominated by quartz, followed by the feldspars, carbonates, pyrite and clay minerals, and the samples only differ in the percentage of certain

minerals (Table 1, Figure 4). The quartz content of the LSL shale (averaging 54.3%) is higher than that of the UOW shale (50.4%) and LCN shale (42.45%). The average contents of feldspar, pyrite and the carbonate minerals in the LCN shale are the highest among the three studied shales. The contents of clay minerals in the LSL and UOW shales have similar values, with averages of 30.0% and 31.7%, respectively, while the LCN shale has an average clay mineral content of 27.4%.
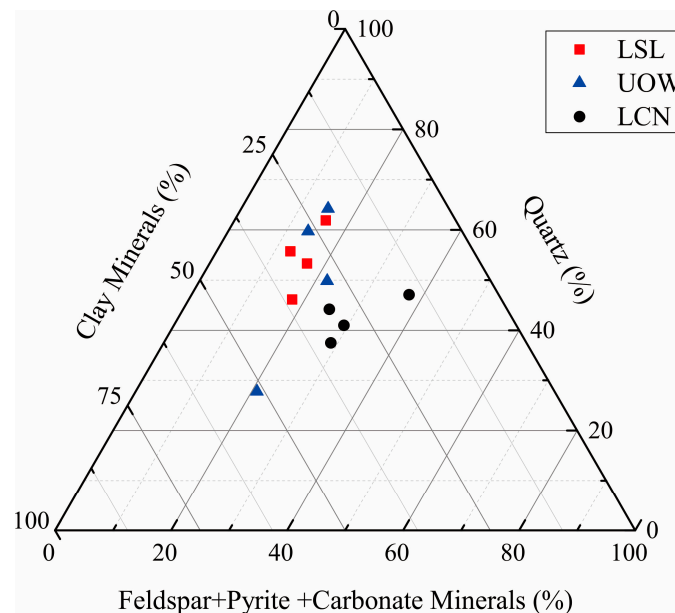


**Figure 4.** The mineral compositions of the collected shale samples.

The brittleness index (BI) is one of the most mechanical properties of gas shale reservoirs regarding hydraulic fracturing during gas exploration [26]. A higher BI index usually indicates a more favorable brittle response and a more developed network of hydraulic fractures in gas shale reservoirs [27]. The sequence of BI values for the investigated shales is LSL shale (averaging 60.8%) > UOW (averaging 56.6%) > LCN (averaging 50.5%) (Table 1), which indicates that the LSL and UOW shales are favorable for implementing hydraulic fracturing when compared with the LCN shale.

*4.2. Petro-Physical Properties of Shale Gas Reservoirs*

4.2.1. Porosity and Permeability

All porosities of the collected samples were lower than 4%, although porosity values vary between the three shales (Table 1). The LSL and UOW shales have noticeably higher porosities (approximately 3%) than the LCN shale (averaging 1.80%). The permeability of the studied shales rank as LSL shale (average of 0.0016 mD) > UOW shale (average of 0.0014 mD) > LCN shale (average of 0.0012 mD) (Table 1). The distinction of the porosity and permeability between different shales in this study is consistent with these previous studies [11,13,17], which indirectly confirms the veracity of the comparison regarding the porosity and permeability of different shales.

The permeability possesses a positive correlation with porosity for the collected shales (Figure 5), indicating that pores are the primary contributors to permeability. Moreover, based on the limited number of samples, the slopes of the three fit lines in Figure 5 show that the porosity contribution to permeability is much more significant in the LSL shale than in the UOW and LCN shales. However, further study is needed to confirm this with enough samples.
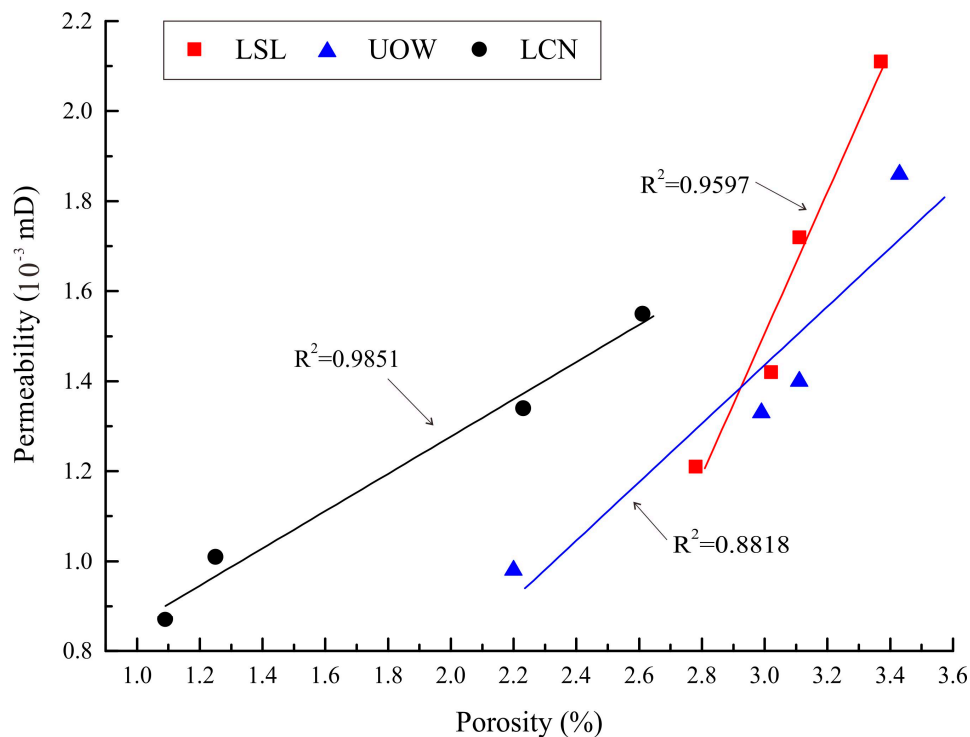
**Figure 5.** Linear relationships between the porosity and permeability of the collected shales.

### 4.2.2. FE-SEM Observation

The results from the FE-SEM analysis indicate that the pores in these shales include inter-particle pores, intra-particle pores and organic matter pores. The inter-particle pores are mainly present at the contacts between mineral grains, such as between quartz, feldspar and pyrite (e.g., Figure 6a,d,g). The intra-particle pores refer to the microscopic pores that exist within minerals and that are especially common in clay minerals (e.g., Figure 6a,g). The organic-matter pores represent the pores related to organic matter, which generally originate from hydrocarbon generation (Figure 6d). The FE-SEM observations illustrate that these pores are less common in the LCN shale compared to LSL and UOW shales (Figure 6), which partially explains the relatively low porosity of the LCN shale.

The SEM images also demonstrate that the micro-fractures in the LCN are not as well developed as those in the LSL and UOW shales. Both the size and quantity of micro-fractures in the LSL shale (Figure 6b,c) and UOW shale (Figure 6e,f) are greater than those in the LCN shale (Figure 6h,i). The less developed fracture system in the LCN shale is responsible for the lower permeability among the collected shales because fractures play a dominant role in gas transport in shales.

**Figure 6.** Images of pores and fractures from the collected shale samples using SEM inter-P (inter-particle pores), intra-P (intra-particle pores), OM-P (organic matter pores): (**a**–**c**) pores and fractures in LSL shale; (**d**–**f**) pores and fractures in UOW shale; (**g**–**i**) pores and fractures in LCN shale.

4.2.3. Pore Size Distribution (PSD)

According to the results of the low-pressure $N_2$ adsorption experiment (Figure 7), the pores in the shale are mainly mesopores (pore diameter of approximately 2–50 nm), with trace amounts of micropores (pore diameter of <2 nm) and macropores (>50 nm). The plots also imply distinctly different PSD for three sample groups of the LSL (Figure 7a), UOW (Figure 7b) and LCN shales (Figure 7c). The maximum value of total pore volumes analyzed by the BJH method is from the LSL shale (Y-L-1, 0.0205 $cm^3/g$), while the minimum value is from the LCN shale (Z-N-2, 0.0007 $cm^3/g$) (Figure 7). Generally, the average total pore volume statistics of all samples suggest the sequence: LSL shale (0.0089 $cm^3/g$) > UOW shale (0.0060 $cm^3/g$) > LCN shale (0.0038 $cm^3/g$). The average total pore volume of the LCN shale is only 0.0013 $cm^3/g$, even if the extremely high value is 0.0113 $cm^3/g$ for P-N-1 (Figure 7).

The PSD performance is consistent with the stronger compaction experienced by the LCN shale because of its much earlier formation, and also partially explains the lower porosity of the LCN shale compared to the LSL and UOW shales. As higher total pore volume is more advantageous for shale gas extraction [17,28], the results of the PSD analysis show that the LSL and the UOW shales are more competitive than the LCN shale.
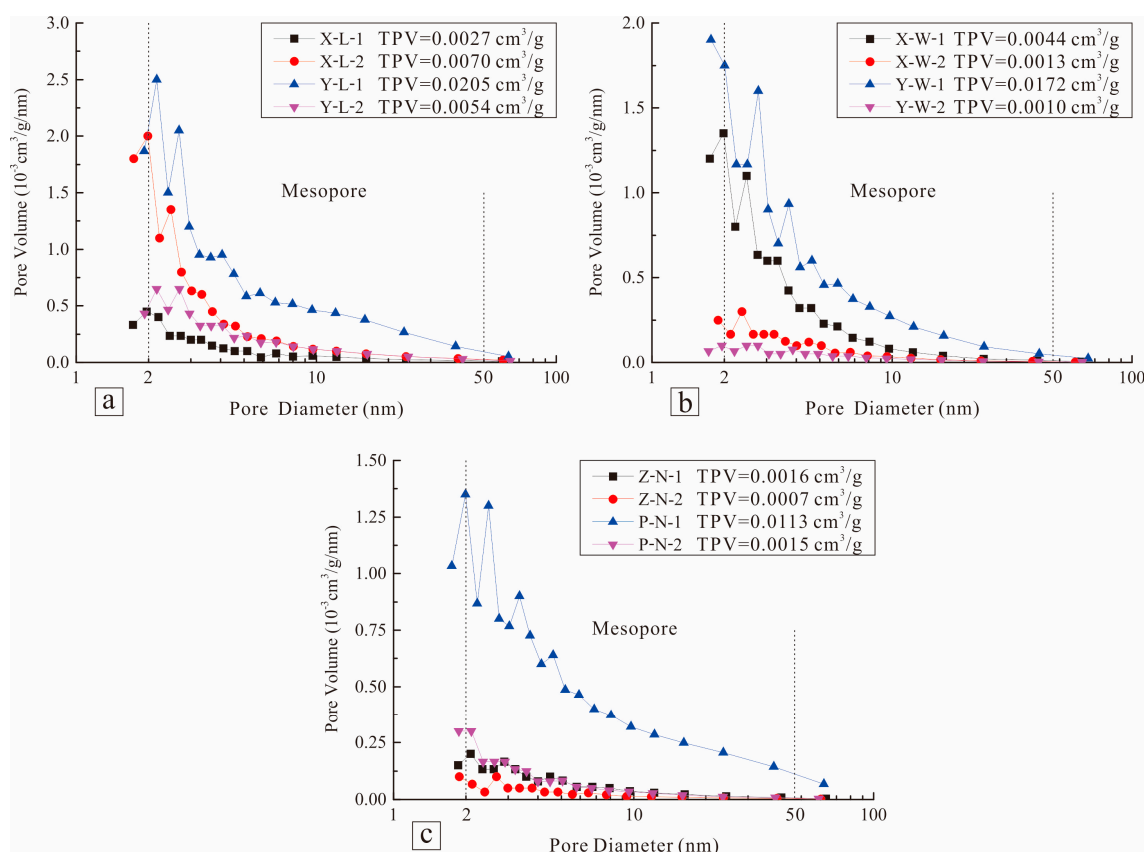
**Figure 7.** Plots of the pore size distribution (PSD) of collected samples derived from the $N_2$ adsorption experiments using the Barrett–Joyner–Halenda (BJH) model. TPV (total pore volume): (**a**) LSL shale; (**b**) UOW shale; (**c**) LCN shale.

### 4.3. TOC Content and Thermal Maturity

The organic fraction in shale, used for TOC characterization, is composed of the residual organic matter after oil generation and expulsion, in addition to the pyrobitumen originating from the cracking of retained oil [29,30]. The TOC content is positively related to the kerogen content of shale samples. Thus, a high TOC content generally indicates a high hydrocarbon potential, and vice versa [31]. The LCN shale has a high TOC content, with an average of 6.16%, compared to the values of 3.55% for the UOW shale and 3.28% for the LSL shale (Table 1; Figure 8). This implies a favorable potential for hydrocarbon generation during the geological interval represented by the LCN shale, compared to that of the LSL and UOW shales.

The average $R_o$ of the LCN shale (4.04%) is also the highest, whereas the $R_o$ of the UOW and LSL shales average 2.76% and 3.10%, respectively (Table 1; Figure 8). This indicates that all of the collected shales are over-mature ($R_o > 2.0\%$), and that the LCN shale is highly over-mature ($R_o > 3.5\%$). Wang et al. [32] observed that some of the organic matter in the LCN shale had been carbonized at a highly over-mature stage. During carbonization, a subset of the organic-matter pores were destroyed or collapsed. This carbonization may partially explain the lower average porosity of the LCN shale.
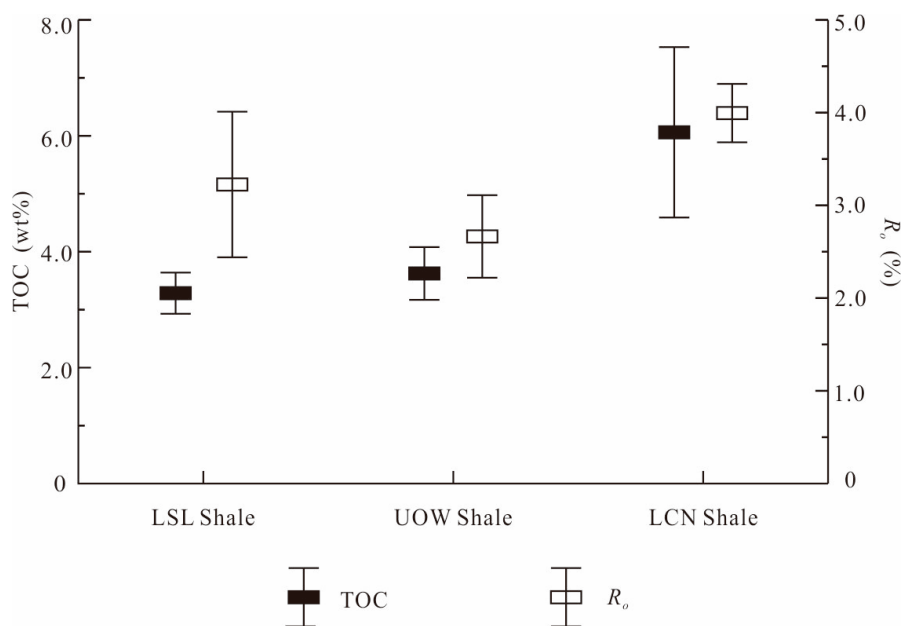
**Figure 8.** A comparison of TOC and $R_o$ among the studied shales.

The value of $R_o$ is related to the geothermal metamorphism of shale (Figure 9). A highly useful parameter to assess oil and gas generation, $R_o$ is directly related to the extent of organic matter conversion [1]. A higher $R_o$ indicates a higher conversion efficiency of organic matter until maximum conversion efficiency [33]. This suggests that the LCN shale experienced more efficient hydrocarbon generation during its history, because it possesses the highest hydrocarbon potential (interpreted from TOC) when compared to the LSL shale and UOW shale, as well as the complete decomposition of organic matter (represented by $R_o$).

### 4.4. Gas-Bearing Properties

#### 4.4.1. In Situ Gas Content and Methane Adsorption Capacity

In situ gas content is one of the most important parameters to evaluate shale gas potential and to find a "sweet point" [34]. The in situ gas content is extremely low in the LCN shale, with an average of 0.91 $m^3$/t (Table 2). In contrast, both the LSL shale and UOW shale have higher gas contents, with average values of 1.82 $m^3$/t and 2.21 $m^3$/t, respectively (Table 2).

**Table 2.** In situ gas contents and gas components in the studied shales.

| Sample ID | Strata | Gas Content ($m^3$/t) | Main Molecular Component (vol %) | | | | | |
|---|---|---|---|---|---|---|---|---|
| | | | $CH_4$ | $C_2H_6$ | $C_3H_8$ | $CO_2$ | $N_2$ | $H_2$ |
| X-L-1 | LSL | 0.95 | 97.39 | 0.42 | 0.01 | 0.78 | 1.31 | 0.03 |
| X-L-2 | LSL | 1.86 | 97.11 | 0.53 | 0.02 | 0.30 | 1.87 | - |
| Y-L-1 | LSL | 1.97 | 94.55 | 0.51 | - | 1.78 | 3.08 | 0.01 |
| Y-L-2 | LSL | 2.49 | 96.01 | 1.23 | 0.02 | 0.44 | 2.27 | - |
| X-W-1 | OUW | 1.41 | 95.55 | 0.37 | 0.03 | 1.16 | 2.84 | - |
| X-W-2 | OUW | 1.59 | 97.26 | 0.70 | - | 0.04 | 1.90 | 0.07 |
| Y-W-1 | OUW | 2.66 | 96.27 | 0.57 | - | 1.05 | 2.07 | - |
| Y-W-2 | OUW | 3.17 | 96.32 | 0.50 | 0.01 | 1.04 | 1.81 | 0.15 |
| Z-N-1 | LCN | 0.49 | 23.17 | 0.08 | - | 16.41 | 56.18 | 2.38 |
| Z-N-2 | LCN | 1.32 | 16.27 | 0.02 | - | 22.80 | 58.48 | 1.08 |

The sorption isotherms of the 12 shale samples are shown in Figure 10, and the Langmuir volumes ($V_L$) for these samples are given in Table 1. The LCN shale has a higher methane adsorption capacity than the LSL and UOW shales. As shown in Figure 11, there is a strong positive correlation between the $V_L$ and TOC content ($R^2 = 0.8273$), but no clear relationship between the $V_L$ and the content of clay minerals. This indicates that the methane adsorption capacity of the shales is mainly related to the organic composition of the shale, and not to the inorganic composition for the samples studied in this work.

As discussed previously, the LCN shale possesses a higher potential for methane adsorption, but the in situ gas content of the LCN shale is extremely low (Table 2). The primary explanation for this is the different burial and thermal evolution histories of the three shales (Figure 9). According to the burial history (Figure 9), the wet gas generation ($R_o$ of 1.3%) of the LCN shale occurred at approximately 420 Ma and the dry gas generation ($R_o$ of 2.0%) began at 250 Ma, while both the wet gas and dry gas generation for the LSL and UOW shales occurred relatively later (from approximately 200–150 Ma) (Figure 9). This likely caused a portion of the hydrocarbon gas generated in the early stage to migrate out of the LCN shale. The possible migration pathways include (1) faults formed by tectonic movement 420–200 Ma [35]; and (2) the unconformable surface between the LCN shale and the Upper Ediacaran Dengying formation. Therefore, we suggest that this relatively early generation of hydrocarbon gas may partially explain why the LCN shale has a lower in situ gas content even though it possesses a greater methane adsorption capacity.
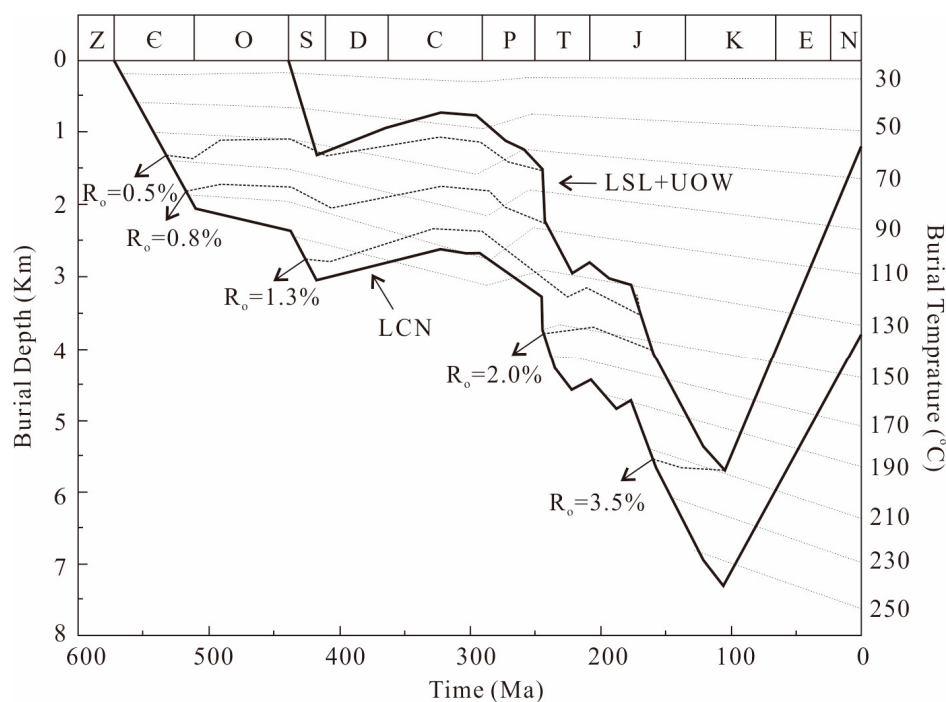


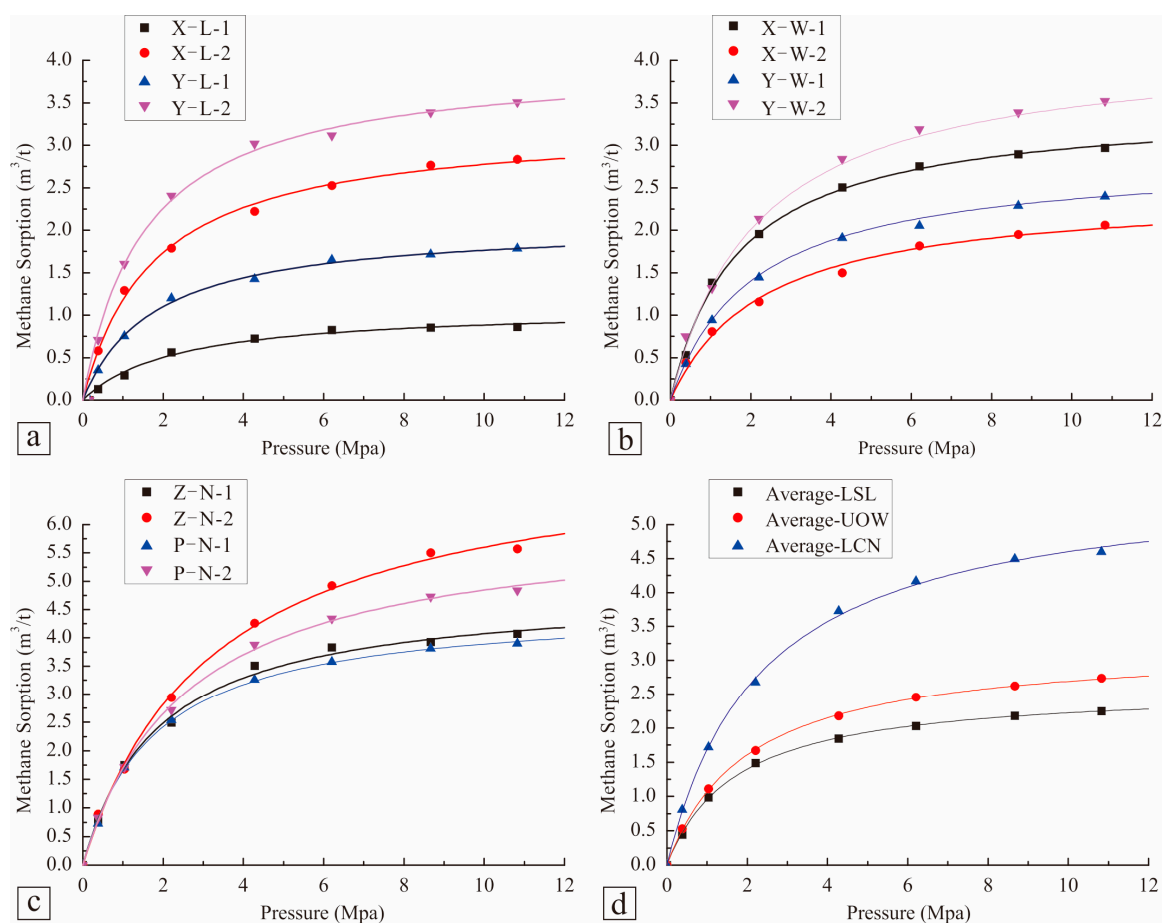**Figure 9.** The burial history of LSL, UOW and LCN in the study area. (Modified from Tao et al. [36]).

**Figure 10.** Langmuir isothermal adsorption curves of the selected shales. (**a**) LSL shale; (**b**) UOW shale; (**c**) LCN shale; (**d**) average statistics.
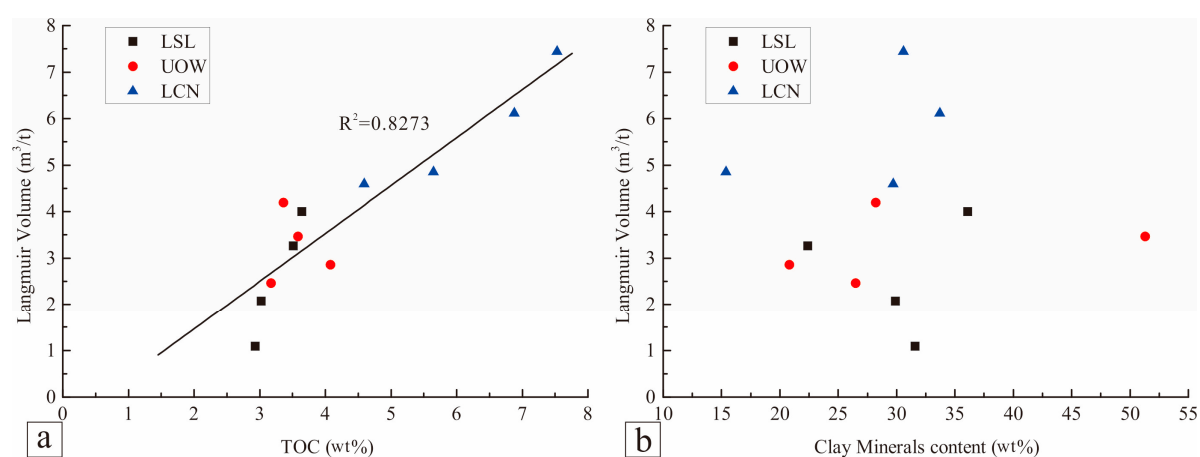


**Figure 11.** Relationships of (**a**) Langmuir volume vs. TOC content; and (**b**) Langmuir volume vs. clay mineral content.

### 4.4.2. Gas Molecular Composition

As shown in Table 2, the molecular components of the desorbed gases in the LSL and UOW shales are predominantly $CH_4$, with some inorganic gases (mainly $CO_2$, $N_2$ and $H_2$). Regarding the major molecular component, the $CH_4$ concentration is generally greater than 94% for the gas samples from the LSL and UOW shales. In contrast, the LCN shale has low $CH_4$, high $CO_2$ (approximately 20%) and extremely high $N_2$ (57.33%). The gas molecular composition data in this study confirms that there was a critical stage of dissipation of the shale gas generated in the LCN shale.

To explain the low-$CH_4$ and high-$N_2$ characteristics of the LCN shale, Wang et al. [37]. indicated that the faults and fractures acted as a migration pathway for the dissipation of $CH_4$ in the shale reservoir. According to Zhu et al. [38], the Upper Ediacaran Dengying formation dolomite (shown in Figure 2) was rich in formation water and other hydrothermal fluids. These Dengying formation fluids could have provided an important medium for the exchange of $CH_4$ in the LCN shale with the $N_2$ from the Dengying formation or from the deeper Earth's upper mantle [37], which is likely the primary reason for high $N_2$ in the LCN shale. The high $CO_2$ content in the LCN shale may be related to the chemical dissolution effects of acidic fluids in the Dengying formation dolomites [38]. The $CO_2$ generated by chemical dissolution can be adsorbed onto the shale due to the higher adsorption capacity of shale for $CO_2$ than for $CH_4$ [39,40]. The continuous dissolution and resorption by the shale resulted in the high $CO_2$ content of the LCN shale.

In addition, the relatively high $CO_2$ and $N_2$ content in the LCN shale also can be the result of ambient air contamination that occurred during gas sampling, even though a sealed coring process was collected. However, gas samplings from different shales were conducted by exactly the same method, thus we state that the measured results can be treated as relatively correct.

### 4.5. Gas Production Potential

To evaluate the gas production potential of the shale reservoir, we considered formation thickness, TOC, $R_o$, porosity, BI and in situ gas content [41,42]. We also compared the three shales with marine shales of North America in Figure 12. The data from the North American shales show that commercial gas production can be achieved in shales with different geological characteristics. For example, the Barnett shale has a high gas content and shale thickness (Figure 12a), and the New Albany shale has extremely high TOC content and high porosity (Figure 12b), while the Ohio shale is fairly favorable in shale thickness and brittleness properties (Figure 12c). The shale data from North America and China confirm that there is a minimum threshold value for commercial shale gas development. In this study, we used the criteria in Wan et al. [43] to evaluate the three investigated shales.

Compared with the North American shales, the investigated shales have a higher maturity but lower porosity. Among the three studied shales, the LSL shale is the most favorable for shale gas development because the values of all considered parameters are superior to the corresponding minimum threshold value (Figure 12d). The UOW shale (Figure 12e) is too thin (with a thickness of approximately 3–10 m) and the LCN shale (Figure 12f) has an extremely low in situ gas content. Thus, both the UOW and LCN shales are unfavorable for individual shale gas production.
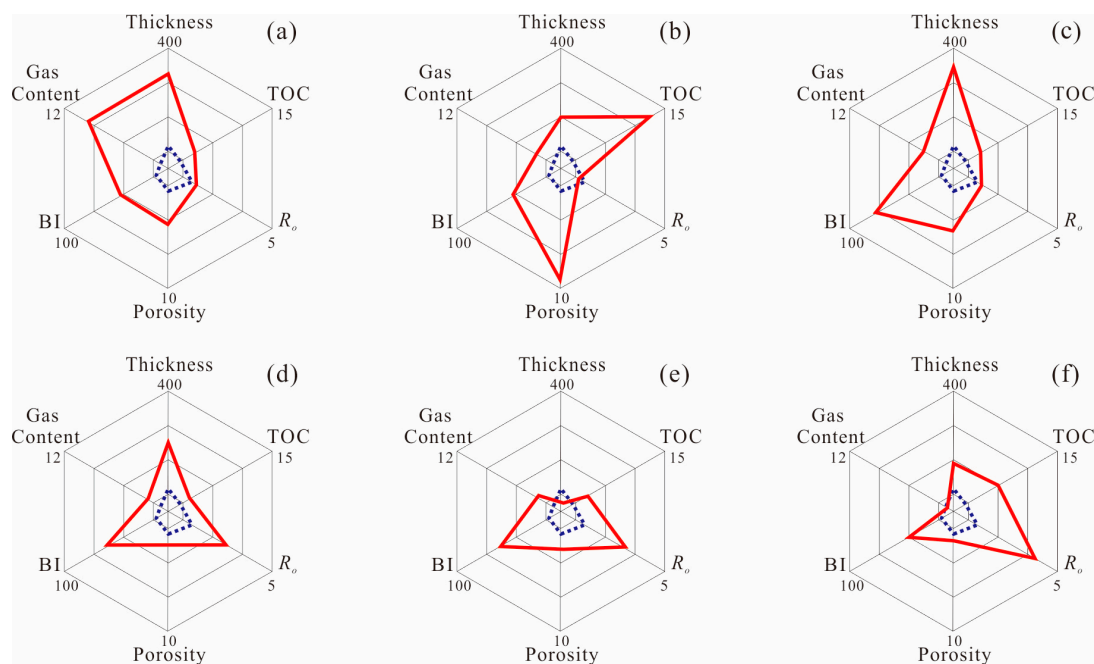
**Figure 12.** Comparison of reservoir properties among the different marine shales. (**a**) Barnett shale; (**b**) New Albany shale; (**c**) Ohio shale; (**d**) LSL shale; (**e**) UOW shale and (**f**) LCN shale. (**a**–**d**) are modified from Curtis [44]. The dotted lines represent the minimal threshold for shale gas development [43].

## 5. Conclusions

We compared the shale gas reservoir characteristics and gas production potential of three key marine shales (LSL, UOW and LCN) in the southeastern margin of the Sichuan Basin. The following conclusions were made.

Compared with the LSL and UOW shales, the LCN shale has the highest TOC content and $R_0$, indicating that the LCN shale likely experienced a more efficient hydrocarbon generation over its history. Compared with the LCN shale, the LSL and UOW shales have favorable brittleness properties for implementing hydraulic fracturing to stimulate the gas flow from the shale bed.

The LSL and UOW shales have higher porosity and permeability than the LCN shale for two reasons: (1) the more developed pores and fracture systems in the LSL and UOW shales are important contributions to permeability; and (2) some organic-matter pores in the LCN shale were damaged or collapsed by the carbonization of organic matter at a highly over-mature stage. This conclusion was confirmed by the PSD results of the low-pressure $N_2$ adsorption analyses of the shale samples.

The LSL and UOW shales have significantly higher gas contents and methane saturation than the LCN shale because of the different burial and thermal evolution of the three shales. The hydrocarbon gas generation of the LCN shale occurred so early that a portion of the generated hydrocarbon gas has migrated out of the reservoir.

After comparison with the gas shale in North America, the LSL shale is the most favorable shale reservoir out of the three studied shales, although the combination of the LSL and UOW shales is also potentially productive. However, the individual single layer production of the UOW or LCN shales is still limited due to its poor resource potential and/or physical characteristics.

## References

1. Jarvie, D.M.; Hill, R.J.; Ruble, T.E.; Pollastro, R.M. Unconventional shale-gas system: The Mississippian Barnett shale on north-center Texas as one model for thermogenic shale-gas assessment. *AAPG Bull.* **2007**, *91*, 475–499. [CrossRef]

2. Vengosha, A.; Warnera, N.; Jacksona, R.; Darraha, T. The effects of shale gas exploration and hydraulic fracturing on the quality of water resources in the United States. *Procedia Earth Planet. Sci.* **2013**, *7*, 863–866. [CrossRef]

3. EIA. 2016. Available online: http://www.eia.gov/todayinenergy/detail.php?id=27512 (accessed on 15 August 2016).

4. Xin, G.; Cole, D.R.; Rother, G.; Mildner, D.F.R.; Brantley, S.L. Pores in Marcellus shale: A neutron scattering and FIB-SEM study. *Energy Fuels* **2015**, *29*, 1295–1308.

5. Dai, J.X.; Dong, D.Z.; Ni, Y.Y.; Wu, W.; Gong, D.Y.; Huang, S. Geochemical characteristics of marine and terrestrial shale gas in China. *Mar. Pet. Geol.* **2016**, *76*, 444–463. [CrossRef]

6. Jing, T.Y.; Zhang, J.C.; Nie, H.K.; Jiang, S.L. Favorable geological conditions for Paleozoic shale gas accumulation in China. *Adv. Mater. Res.* **2013**, *868*, 181–185. [CrossRef]

7. Zhao, X.G.; Yang, Y.H. The current situation of shale gas in Sichuan, China. *Renew. Sustain. Energy Rev.* **2015**, *50*, 653–664.

8. Jiang, S.; Tang, X.L.; Cai, D.S.; Xue, G.; He, Z.L.; Long, S.X.; Peng, Y.M.; Gao, B.; Xu, Z.Y.; Dahdah, N. Comparison of marine, transitional, and lacustrine shales: A case study from the Sichuan Basin in China. *J. Pet. Sci. Eng.* **2017**, *150*, 334–347. [CrossRef]

9. Jiang, Z.X.; Guo, L.; Liang, C. Lithofacies and sedimentary characteristics of the Silurian Longmaxi shale in the Southeastern Sichuan Basin, China. *J. Palaeogeogr.* **2013**, *2*, 238–251.

10. Liu, J.; Yao, Y.B.; Elsworth, D.; Pan, Z.J.; Sun, X.X.; Ao, W.H. Sedimentary characteristics of the lower Cambrian Niutitang shale in the southeast margin of Sichuan Basin, China. *J. Nat. Gas Sci. Eng.* **2016**, *36*, 1140–1150. [CrossRef]

11. Dai, J.X.; Zou, C.N.; Liao, S.M.; Dong, D.Z.; Ni, Y.Y.; Huang, J.L.; Wu, W.; Gong, D.Y.; Huang, S.P.; Hu, G.Y. Geochemistry of the extremely high thermal maturity Longmaxi shale gas, Southern Sichuan Basin. *Org. Geochem.* **2014**, *74*, 3–12. [CrossRef]

12. Sun, M.D.; Yu, B.S.; Hu, Q.H.; Chen, S.; Xia, W.; Ye, R.C. Nanoscale pore characteristics of the Lower Cambrian Niutitang formation shale: A case study from well Yuke #1 in the southeast of Chongqing, China. *Int. J. Coal Geol.* **2015**, *154*, 16–29.

13. Qu, H.Y.; Pan, Z.J.; Peng, Y.; Zhou, F.J. Controls on matrix permeability of shale samples from Longmaxi and Niutitang formations, China. *J. Nat. Gas Sci. Eng.* **2016**, *33*, 599–610. [CrossRef]

14. Yang, R.; He, S.; Hu, Q.H.; Hu, D.F.; Zhang, S.W.; Yi, J.Z. Pore characterization and methane sorption capacity of over-mature organic-rich Wufeng and Longmaxi shales in the Southeast Sichuan Basin, China. *Mar. Pet. Geol.* **2016**, *77*, 247–261. [CrossRef]

15. Ma, Y.; Pan, Z.J.; Zhong, N.N.; Connell, L.D.; Down, D.I.; Lin, W.L.; Zhang, L. Experimental study of anisotropic gas permeability and its relationship with fracture structure of Longmaxi shales, Sichuan Basin, China. *Fuel* **2016**, *180*, 106–115. [CrossRef]

16. Han, C.; Jiang, Z.X.; Han, M.; Wu, M.H.; Lin, W. The lithofacies and reservoir characteristics of the Upper Ordovician and Lower Silurian black shale in the Southern Sichuan Basin and its periphery, China. *Mar. Pet. Geol.* **2016**, *75*, 181–191. [CrossRef]

17. Tian, H.; Pan, L.; Zhang, T.W.; Xiao, X.M.; Meng, Z.P.; Huang, B. Pore characterization of organic-rich Lower Cambrian shales in Qiannan Depression of Guizhou Province, Southwestern China. *J. Mar. Pet. Geol.* **2015**, *62*, 28–43. [CrossRef]

18. Gai, S.H.; Liu, H.Q.; He, S.L.; Mo, S.Y.; Chen, S.; Liu, R.H.; Huang, X.; Tian, J.; Lv, X.C.; Wu, D.X.; et al. Shale reservoir characteristics and exploration potential in the target: A case study in the Longmaxi formation from the Southern Sichuan Basin of China. *J. Nat. Gas Sci. Eng.* **2016**, *31*, 86–97. [CrossRef]

19. Korsch, R.J.; Mai, H.; Sun, Z.; Gorter, J.D. The Sichuan Basin, southwest China—A Late Proterozoic (Sinian) petroleum province. *Precambrian Res.* **1991**, *54*, 45–63. [CrossRef]

20. Tian, L.; Wang, Z.M.; Krupnick, A.; Liu, X.L. Stimulating shale gas development in China: A comparison with the US experience. *Energy Policy* **2014**, *75*, 109–116. [CrossRef]

21. Chen, L.; Lu, Y.C.; Jiang, S.; Li, J.Q.; Guo, T.L.; Luo, C.; Xing, F.C. Sequence stratigraphy and its application in marine shale gas exploration: A case study of the Lower Silurian Longmaxi formation in the Jiaoshiba shale gas field and its adjacent area in Southeast Sichuan Basin, SW China. *J. Nat. Gas Sci. Eng.* **2015**, *27*, 410–423. [CrossRef]

22. Chen, Z.M.; Yong, Z.Q.; Zhu, J.P.; Xin-Min, Y.E.; Hao, W.; Shuang, Z. Features of Wufeng formation and Longmaxi formation shale in Nanchuan, southeast of Sichuan, China. *J. Chengdu Univ. Technol.* **2013**, *40*, 696–702. (In Chinese)

23. Hartman, R.C.; Ambrose, R.J.; Akkutlu, I.Y. Shale gas-in-place calculations Part II—Multicomponent gas adsorption. In Proceedings of the SPE Unconventional Gas Conference, Woodlands, TX, USA, 14–16 June 2011; pp. 14–15.

24. Chalmers, G.R.L.; Bustin, R.M. Lower Cretaceous gas shales in northeastern British Columbia, Part I: Geological controls on methane sorption capacity. *Bull. Can. Pet. Geol.* **2008**, *56*, 1–21. [CrossRef]

25. Jacob, H. Dispersed solid bitumens as an indicator for migration and maturity in prospecting for oil and gas. *Erdöl Kohle Erdgas Petrochem.* **1985**, *38*, 365–392.

26. Rickman, R.; Mullen, M.J.; Petre, J.E.; Grieser, W.V.; Kundert, D. A practical use of shale petrophysics for stimulation design optimization: All shale plays are not clones of the Barnett shale. In Proceedings of the SPE Annual Technical Conference and Exhibition, Denver, CO, USA, 21–24 September 2008; pp. 21–24.

27. Gale, F. Screening criteria for shale-gas systems. *Gulf Coast Assoc. Geol. Soc. Trans.* **2009**, *59*, 779–793.

28. Grathoff, G.H.; Peltz, M.; Enzmann, F.; Kaufhold, S. Porosity and permeability determination of organic-rich Posidonia shales based on 3-D analyses by FIB-SEM microscopy. *Solid Earth Discuss.* **2016**, *7*, 1145–1156. [CrossRef]

29. Ross, D.J.K.; Bustin, R.M. The importance of shale composition and pore structure upon gas storage potential of shale gas reservoirs. *Mar. Pet. Geol.* **2009**, *26*, 916–927. [CrossRef]

30. Bernard, S.; Wirth, R.; Schreiber, A.; Schulz, H.M.; Horsfield, B. Formation of nanoporous pyrobitumen residues during maturation of the Barnett Shale (Fort Worth Basin). *Int. J. Coal Geol.* **2012**, *103*, 3–11. [CrossRef]

31. Xue, H.Q.; Jiang, P.X.; Xu, R.N.; Zhao, B.; Zhou, S.W. Comparison of marine, transitional, and lacustrine shales: A case study from the Sichuan Basin in China. *J. Nat. Gas Sci. Eng.* **2016**, *29*, 150–159. [CrossRef]

32. Wang, Y.F.; Leng, J.G.; Li, P.; Li, F. Characteristics and its main enrichment controlling factors of shale gas of the Lower Cambrian Niutitang formation in northeastern Guizhou Province. *J. Palaeogeogr.* **2016**, *18*, 605–614, (In Chinese with English Abstract).

33. Cheng, P.; Xiao, X.M.J. Gas content of organic-rich shales with very high maturities. *J. China Coal Soc.* **2013**, *38*, 737–741. (In Chinese)

34. Sondergeld, C.H.; Newsham, K.E.; Comisky, J.T.; Rice, M.C.; Rai, C.S. Petrophysical considerations in evaluating and producing shale gas resources. In Proceedings of the SPE Unconventional Gas Conference, Pittsburgh, PA, USA, 23–25 February 2010; pp. 23–25.

35. Zhu, C.Q.; Xu, M.; Shan, J.N.; Yuan, Y.S.; Zhao, Y.Q.; Hu, S.B. Quantifying the denudations of major tectonic events in Sichuan Basin: Constrained by the paleothermal records. *Geol. China* **2009**, *36*, 1268–1277. (In Chinese)

36. Tao, S.; Tang, D.Z.; Xu, H.; Yang, F.; Zhou, C.W.; Li, S. The analysis for thermal evolution history of high–over mature source rock from Cambrian to Silurian in Upper- Middle Yangtze Region. *Prog. Nat. Sci.* **2009**, *19*, 1126–1133. (In Chinese)

37. Wang, R.Y.; Ding, W.L.; Gong, D.J.; Leng, J.G.; Wang, X.H.; Yin, S.; Sun, Y.X. Gas preservation conditions of marine shale in Northern Guizhou area: A case study of the Lower Cambrian Niutitang formation in the Cen'gong block, Guizhou Province. *Oil Gas Geol.* **2016**, *37*, 45–55. (In Chinese)

38. Zhu, D.Y.; Zhang, D.W.; Zhang, R.Q.; Feng, J.F.; He, Z.L. Fluid alteration mechanism of dolomite reservoirs in Dengying formation, south China. *Acta Pet. Sin.* **2015**, *36*, 1188–1198. (In Chinese)

39. Fathi, E.; Akkutlu, I.Y. Multi-component gas transport and adsorption effects during $CO_2$ injection and enhanced shale gas recovery. *Int. J. Coal Geol.* **2014**, *123*, 52–61. [CrossRef]

40. Godec, M.; Koperna, G.; Petrusak, R.; Oudinot, A. Enhanced Gas Recovery and $CO_2$ Storage in Gas Shale: A Summary Review of its Status and Potential. *Energy Procedia* **2014**, *63*, 5849–5857. [CrossRef]

41. Montgomery, S.; Jarvie, D.; Bowker, K.; Pollastro, R. Mississippian Barnett Shale, Fort Worth Basin, north-central Texas: Gas-shale play with multi-trillion cubic foot potential. *Precambrian Res.* **2005**, *89*, 155–175. [CrossRef]

42. Yang, F.; Ning, Z.F.; Zhang, R.; Zhao, H.W.; Krooss, B.M. Investigations on the methane sorption capacity of marine shales from Sichuan Basin, China. *Int. J. Coal Geol.* **2015**, *146*, 104–117. [CrossRef]

43. Wan, Y.; Tang, S.H.; Pan, Z.J. Evaluation of the shale gas potential of the Lower Silurian Longmaxi formation in Northwest Hunan Province, China. *Mar. Pet. Geol.* **2017**, *79*, 159–175. [CrossRef]

44. Curtis, J.B. Fractured shale-gas systems. *AAPG Bull.* **2002**, *86*, 1921–1938.